

Research Article

Thermophoresis & Soret-DuFour on MHD Mixed Convection of a Nano Fluid with a Porous Medium over a Stretching Sheet with a Non-Uniform Heat Source/Sink

Prashanth Manthramurthy^{*} , Srinivasa Rao

Department of Mathematics, Anurag University, Hyderabad, India

Abstract

This work aimed to examine the effects of thermal diffusion (Soret) and diffusion-thermo (DuFour) on MHD mixed convective flow of a viscous nanofluid across a stretching sheet under a magnetic field embedded in a porous medium in the presence of non-uniform heat source/sink and chemical reaction. The governing equations are transformed into a set of ordinary differential equations using the similarity transformation approach. They are subsequently resolved computationally by use of the efficient Keller box method. The effects of different physical factors on concentration, temperature, and velocity profiles are graphically shown. Increasing Du values decreases temperature, although concentration profiles indicate the reverse. As temperature rises, the chemical reaction parameter Kr values increase, while the concentration profile decreases. The temperature was found to rise when the space-dependent (A1) and temperature-dependent (B1) parameters for heat source/sink increased. Additionally, a tabular presentation of the skin friction coefficient, Nusselt number, and Sherwood number behaviour is provided. Mixed convection heat and mass transfer flows are very important in manufacturing for designing reliable equipment, nuclear power plants, gas turbines, and various propulsion devices for aircraft, rockets, satellites, and spacecraft. The effects of non-uniform heat sources/sinks, thermophoresis, and chemical reactions on mixed convection flow play an important role in space technology and high-temperature processes.

Keywords

MHD, Soret, DuFour, Mixed Convention, Non-Uniform Heat Source/Sink, Chemical Reaction

1. Introduction

Magneto-hydrodynamics (MHD) is the study of the movement of an electrically conducting fluid in the presence of a magnetic field. The Joule heating enters the energy equation in the MHD linked to the heat transfer problem, along with the additional body force term, or Lorentz force. Because it has many practical applications in geophysical and astrophysical phenomena, including stellar and planetary processes, the study of MHD of viscous electrically conduct-

ing fluids is important. Radiation is the term used to describe the transfer of energy using electromagnetic waves. When charged particles in matter move thermally, electromagnetic radiation is produced. This is known as thermal radiation. Heat transfer in radiation does not require an intermediary medium, whereas conduction and convection require a medium for heat transfer. A "mass transfer" occurs when there is a change in a mixture's species concentration, which results in the transfer

^{*}Corresponding author: 21hs303103@anurag.edu.in (Prashanth Manthramurthy)

Received: 26 May 2024; **Accepted:** 24 June 2024; **Published:** 15 August 2024



Copyright: © The Author(s), 2024. Published by Science Publishing Group. This is an **Open Access** article, distributed under the terms of the Creative Commons Attribution 4.0 License (<http://creativecommons.org/licenses/by/4.0/>), which permits unrestricted use, distribution and reproduction in any medium, provided the original work is properly cited.

of mass. In everyday life, mass transfer is frequently observed in processes like drying and evaporation, water vapour transfer into dry air, and smoke diffusion into the environment through towering chimneys. Convective mass transfer and diffusion mass transfer are the two distinct forms of mass transfer. Forced and natural convection combine to form mixed convection. Where buoyancy forces are present, we infer forced convection. Examples include the circulation of blood in heated animals, the shock waves produced by explosions, and convection ovens. A solid matrix with a network of linked voids is what is known as a porous media. Examples of porous medium domains include soil, sand, fissured rock, karstic limestone, ceramics, bread, lungs, kidneys, aquifers from which groundwater is pumped, reservoirs that produce oil and/or gas, sand filters for purifying water, packed beds in the chemical engineering sector, and the root zone in agriculture.

Crane [1] discovered an accurate solution by examining the flow caused by a stretching plate whose velocity is proportionate to the distance from a slit. Following up on Crane's ground-breaking breakthrough, numerous scientists expanded on it in a variety of ways for viscous fluids on a stretching sheet, such as Takhar [2] examined the flow and mass distortion of chemical species undergoing first and higher-order reactions across a continually stretched sheet under the influence of an applied magnetic field. Hayat and Javed [3] have generalized three-dimensional MHD flow over a porous stretched sheet. Krishnaiah et al. [4] discovered numerical solutions for a class of nonlinear differential equations that arise in the heat and mass transport of a non-Newtonian fluid towards an exponentially extending surface. The behaviour of non-Newtonian fluids is characterized by the Casson fluid model. Konda et al. [5] examined the flow of melting heat transfer through a porous media that contains thermal radiation as a stretching sheet. Gangadhar and Suneetha [6] studied the Soret and DuFour effects of a two-dimensional, stable, viscous, incompressible, electrically conducting, and laminar MHD free convection flow in the presence of a porous media and heat generation/absorption. Pal and Mondal [7] investigated the transfer of heat and mass through natural convection over a stretching sheet immersed in a fluid-saturated porous medium under a uniform transverse magnetic field in the presence of variable thermal conductivity, Soret and DuFour effects, thermal radiation, viscous dissipation, non-uniform heat source/sink, and temperature-dependent variable viscosity. Patil [8] examined the combined effects of a magnetic field and cross-diffusion on mixed convection flow across an exponentially stretched sheet. Thumma and Mishra [9] looked into how non-uniform heat sources and sinks, as well as Joule and viscous dissipation under velocity slip, convective surface temperature, and zero mass flux circumstances, affect the formation of the 3D Eyring–Powell fluid system in the field of fluid dynamics. Karim et al. [10] studied the DuFour and Soret effects of thermal radiation and an electrically conducting viscous incompressible fluid interaction on the flow over an

inclined linearly stretched sheet in the presence of mass transfer and heat allowed by a transversely applied uniform magnetic field, with heat generation accounting for the Roseland diffusion approximation. Mondal et al. [11] examined the mass transfer of a semi-infinite permeable inclined flat plate in the presence of a non-uniform heat source/sink and chemical reaction, as well as thermophoresis and Soret-DuFour on MHD mixed convective heat. Kalyani et al. [12] looked into the impacts of thermal diffusion, heat source/sink effects, and magnetohydrodynamics on coupled free-forced convection and mass transfer flow across a semi-infinite vertical porous flat plate embedded in a porous medium. Aastha and Chand [13] examined the heat-generating and chemically reacting nanofluid's free convective flow with mass transfer via a vertically moving porous plate in a conducting field, accounting for the Soret and DuFour effects as well as the viscous dissipation effect. Ramadevi et al. [14] examined using three-dimensional (3D) computer modeling the magnetohydrodynamic (MHD) Carreau fluid flow, controlled by a stretching surface affected by mass and heat transfer. Variable thermal conductivity, Joule heating, irregular heat source/sink, and chemical reaction. Hayat et al. [15] examined the properties of flow and heat transmission through a stretching cylinder submerged in a thermally stratified medium. In addition, the effects of thermal radiation and uneven heat generation are taken into account. Ali et al. [16] investigated Soret effects, Hall and MHD effects, and constant free convective mass transport over a vertical porous plate with heat generation. Seth, Tripathi, & Rashidi [17] investigated the effects of diffusion-thermo and thermodiffusion on MHD natural convection flow of an incompressible, heat-absorbing, viscous fluid that conducts electricity and has variable mass and heat fluxes near an inclined stretching sheet in a non-Darcy porous medium while accounting for chemical reaction. Sheikh [18] discovered the analytical solution for the flow of a viscous MHD fluid across a porous oscillatory stretching sheet when thermophoresis is present. Reddy & Chamkha [19] investigated the properties of heat and mass transfer of nanofluids based on Al_2O_3 and TiO_2 over a stretched sheet through a porous media in the presence of radiation, chemical reaction, magnetic field, thermo-diffusion and diffusion-thermo effects, and heat generation/absorption. Ragupathi et al. [20] looked into the possibility of comparing the $\text{Fe}_3\text{O}_4/\text{Al}_2\text{O}_3$ nanoparticle with $\text{H}_2\text{O}/\text{NaC}_6\text{H}_5\text{O}_7$ based nanofluids on the Riga plate with non-uniform heat source-sink effects to get distinct results. Koli and Salunkhe [21] focused on the combined effects of heat radiation and magnetic field on convective nanofluid flow towards a permeable stretched sheet in the presence of suction/injection, thermophoresis, and Brownian motion effects. Lakshmi et al. [22] investigated the effects of uniform transverse magnetic field and non-uniform heat source/sink on Sisko fluid flow across a non-linear stretched sheet. Reddy et al. [23] analyzed the heat and mass transfer of an unsteady magneto-hydrodynamic hybrid nano liquid flow over a stretching/shrinking surface with chemical reaction, suction,

slip effects, and thermal radiation. Water is considered the base fluid, and a combination of alumina (Al_2O_3) and titanium oxide (TiO_2) nanoparticles is considered a hybrid nanoparticle.

The current work aims to investigate the effects of thermal diffusion (Soret) and diffusion-thermo (DuFour) on MHD mixed convective flow of a viscous nanofluid across a stretching sheet in the presence of non-uniform heat source/sink and chemical reaction embedded in a porous medium under a magnetic field. Using the appropriate similarity transformations, the set of dimensional partial differential equations is converted into dimensionless ordinary differential equations, which are then solved numerically using the Keller box method. Graphs and tables are used to illustrate and discuss the results that were collected.

2. Flow of Governing Equations

This study examines the heat radiation soret and DuFour effect of MHD mixed convection of incompressible viscous nanofluid across a stretching sheet with a non-uniform heat

source/sink and chemical reaction on a two-dimensional stable electrically conducting nonlinearly permeable sheet. Figure 1 shows the shape of this flow. This study's investigation takes into account the following suppositions:"

- 1) The problem's geometry is assumed to be represented by a coordinate system with a perpendicular Y-axis and a horizontal X-axis.
- 2) We explore the flow through a stretched sheet of a two-dimensional barrier layer.
- 3) We studied the flow of nanofluids at $y \geq 0$ (the observed coordinate normal to the stretched surface) in the presence of a magnetic field.
- 4) At the boundary, the temperature T and volume concentration C of the nanoparticles are considered to be T_w and C_w at the wall, and T_∞ and C_∞ at a distance from the wall.
- 5) Furthermore, it is hypothesized that when a linear function is utilized, there will be a decrease in temperature gradient in the viscous fluid flow. Using Taylor's technique, the expansion T^4 of moves towards a temperature of free stream T_∞

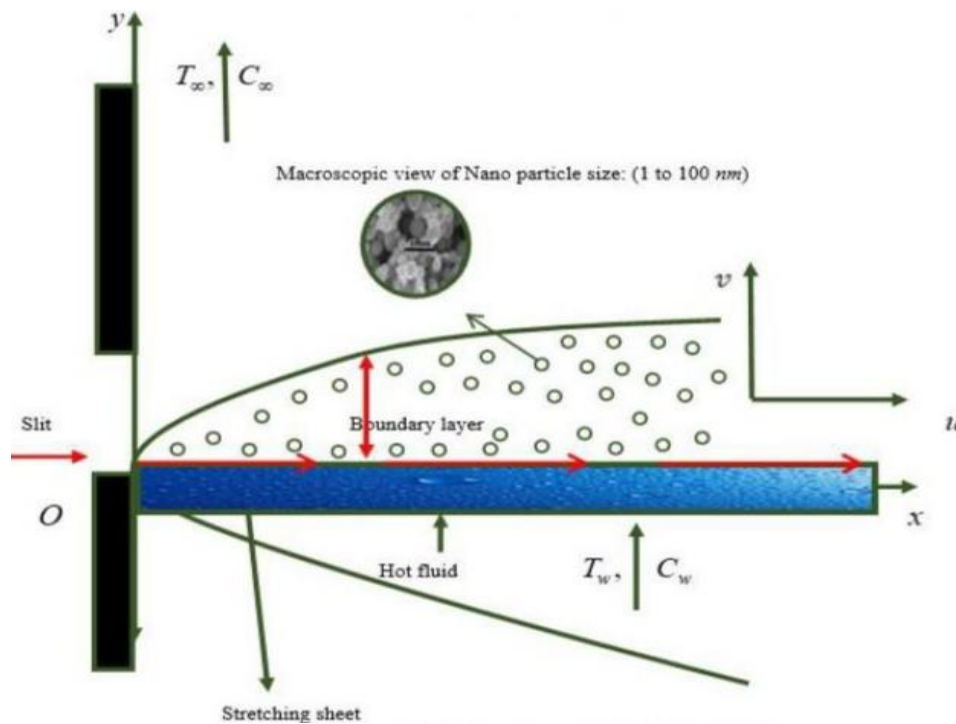


Figure 1. Geometry of the problem.

Governing equations of the problem (Chandu. M. Koli and S. N. Salunkhe [21])

Continuity Equation

$$\frac{\partial u}{\partial x} + \frac{\partial v}{\partial y} = 0 \quad (1)$$

Equation of Momentum

$$\left(\frac{\partial u}{\partial x}\right)u + v\left(\frac{\partial u}{\partial y}\right) = v\left(\frac{\partial^2 u}{\partial y^2}\right) - u\left(\frac{\sigma B^2}{\rho}\right) + g\beta_T[T - T_\infty] + g\beta_C[C - C_\infty] - \frac{v}{K_1}u \quad (2)$$

Equation of Energy

$$u \left(\frac{\partial T}{\partial x} \right) + v \left(\frac{\partial T}{\partial y} \right) = \alpha \left(\frac{\partial^2 T}{\partial y^2} \right) + \tau_B (D_B \left(\frac{\partial c}{\partial y} \right) \left(\frac{\partial T}{\partial y} \right) + \frac{D_T}{T_\infty} \left(\frac{\partial T}{\partial y} \right)^2 + \left(\frac{16 \sigma^* T_\infty^3}{3 K^* \rho C_p} \right) \left(\frac{\partial^2 T}{\partial y^2} \right) + \frac{D_B K_T}{C_s C_p} \left(\frac{\partial^2 c}{\partial y^2} \right) + q''' \quad (3)$$

Where $q''' = \frac{K u_w}{x v} [A_1 [T_w - T_\infty] f' + B_1 [T - T_\infty]]$

Equation of Species nanoparticle volume concentration

$$\left(\frac{\partial c}{\partial x} \right) u + \left(\frac{\partial c}{\partial y} \right) v = D_B \frac{\partial^2 c}{\partial y^2} + \frac{D_T}{T_\infty} \left(\frac{\partial^2 T}{\partial y^2} \right) - K [C - C_\infty] \quad (4)$$

Boundary conditions

$$u_w(x) = U_w \exp\left(\frac{x}{L}\right), v_w(x) = V_0 \exp\left(\frac{x}{2L}\right), T = T_w, \\ C = C_w \text{ at } y = 0 \quad (5)$$

$u \rightarrow 0, v \rightarrow 0, T \rightarrow T_\infty, C \rightarrow C_\infty$ as $y \rightarrow \infty$

Transformation of similarity is presented

$$u = U_0 \exp\left(\frac{x}{L}\right) f'(\eta), v = -\sqrt{\frac{v u_0}{2L}} \exp\left(\frac{x}{2L}\right) \{f(\eta) + \eta f'(\eta)\} \quad (6)$$

$$\eta = y \sqrt{\frac{U_0}{2VL}} \exp\left(\frac{x}{2L}\right), \theta = \frac{T - T_\infty}{T_w - T_\infty}, \phi = \frac{C - C_\infty}{C_w - C_\infty}, T_w - T_\infty = T_0 e^{x/2L}, C_w - C_\infty = C_0 e^{x/2L}$$

When Eq. (6) is applied, the equation of continuity is fulfilled in the same way, and both Eqs. (2) to (4) and (6) have the same form.

$$f'''' - 2(f')^2 + ff'' + G_r \theta + G_c \phi - (M + K)f' = 0 \quad (7)$$

$$\left(1 + \frac{4}{3}R\right)\theta'' + P_r f \theta' - P_r f' \theta + P_r N_b \theta' \phi' + P_r N_t (\theta')^2 + P_r D_u \phi' + P_r \lambda (A_1 f' + B_1 \theta) = 0 \quad (8)$$

$$N_b \phi'' + N_t \theta'' + L_e P_r N_b f \phi' - L_e P_r N_b \phi f' - K_1 L_e P_r N_b \phi = 0 \quad (9)$$

“The corresponding boundary conditions (5) to transform into

$$f(0) = S, f'(0) = \lambda, \theta(0) = 1, \phi(0) = 1 \quad (10)$$

$$f'(\infty) \rightarrow 0, \theta(\infty) \rightarrow 0, \phi(\infty) \rightarrow 0$$

Here physical parameters involved are specified

$$M = \frac{2\sigma B_0^2 L}{\rho U_0}, \lambda = \frac{U_w}{U_0}, P_r = \frac{v}{\alpha}, R = \frac{4\sigma^* T_\infty^3}{3kk^*}, \\ N_b = \frac{(\rho C)_p D_B (C_w - C_\infty)}{v(\rho C)_f}, N_t = \frac{(\rho C)_p D_T (T_w - T_\infty)}{v(\rho C)_f}$$

$$B = B_0 e^{\left(\frac{x}{2L}\right)}, D_u = \frac{D_B K_T (C_w - C_\infty)}{C_s C_p v (T_w - T_\infty)}, K_1 = \frac{2KL}{U_0 e^{\frac{2x}{L}}}, L_e = \frac{\alpha}{D_B}, u_w(x) = U_w \exp\left(\frac{x}{L}\right),$$

$$K = \frac{2VL}{K_1 U_0 e^L} \quad (11)$$

The important physical values are the skin friction coefficients' physical parameters, the local share wood number, and the local Nusselt number.”

$$C_f = \frac{\tau_w}{\rho U_w} \Rightarrow Re_x^{-1/2} C_f = f^{11}(0) \quad (12)$$

$$Nu_x = \frac{x q_w}{k(T_w - T_\infty)} \text{ where } q_w = -\left(k + \frac{16\sigma^* T_\infty^3}{3k^*}\right) \left(\frac{\partial T}{\partial y}\right)_{y=0} \Rightarrow \\ Re_x^{-1/2} Nu_x = -\left(1 + \frac{4R}{3}\right) \theta^1(0) \quad (13)$$

$$Sh_x = \frac{x q_w}{D_B (T_w - T_\infty)} \text{ where } q_w = -D_B \left(\frac{\partial C}{\partial y}\right)_{y=0} \Rightarrow \\ Re_x^{-1/2} Sh_x = -\phi^1(0) \quad (14)$$

Where $Re_x = \frac{U_0 x (\exp(\frac{x}{L}))}{v}$ be the local Reynolds number

3. Keller Box Method

The Keller box method is an implicit unconditionally stable technique capable of solving a variety of different engineering problems. The Keller box method includes the following steps:

- 1) To compute the approximate solution, first write the governing equations into a first-order system of equations.
- 2) The domain is then discretized, allowing for calculation over each subdomain rather than the complete domain. This produces more precise outcomes.
- 3) To get finite difference equations, central-difference derivatives and the average of function midpoints are utilised.
- 4) The resultant equations are then linearized using Newton's approach, as Keller described. Also, write them in a tridiagonal matrix.

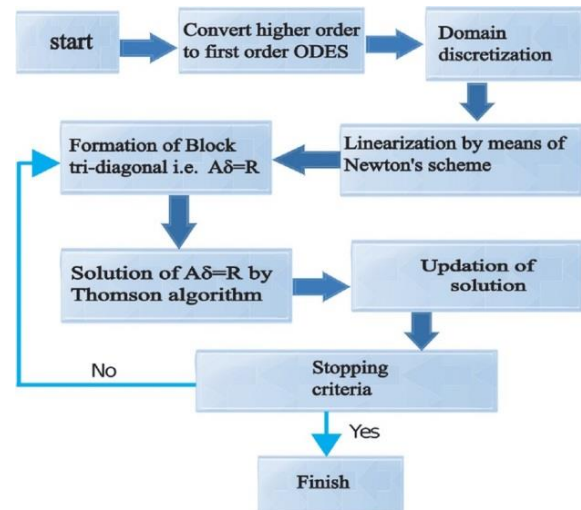


Figure 2. Problem solution in Flow chart format.

Finally, the ultimate result is obtained by using LU decomposition.

Equations (7) - (9) subject to boundary conditions (10) are solved numerically using the Keller box method.

We start with introducing new independent variables

$$\text{Let } f^l = p, p^l = q$$

$$\theta^l = g \quad (\theta = v), g^l = \theta^l,$$

$$\phi^l = \eta \quad (\phi = S), \eta^l = \phi^l$$

$$f^l = p$$

$$p^l = q \Rightarrow f^l = q \Rightarrow f^{ll} = q^l$$

$$\theta^l = g$$

$$\phi^l = \eta \Rightarrow \phi^{ll} = \eta^l$$

$$q^l + f q + G_r \theta + G_c \phi - 2p^2 - (M + K)p = 0$$

$$(1 + \frac{4}{3} R)g^l + \text{Pr } f g - \text{Pr } p \theta + \text{Pr } Nb g \cdot \eta + \text{Pr } Nt g^2 + \text{Pr } Du \eta + Pr \lambda (A_1 p + B_1 \theta) = 0$$

$$Nb \eta^l + Nt g^l + Le \text{Pr } Nb f \eta - Le \text{Pr } Nb p \phi - K_1 Le \text{Pr } Nb \phi = 0$$

$$f(0) = 0, V(0) = 1, P(0) = \lambda, S(0) = 1$$

$$p(\eta) \rightarrow 0, V(\eta) \rightarrow 0, S(\eta) \rightarrow 0 \text{ as } \eta \rightarrow \infty$$

$$f^l = p$$

$$(r_1)_{j-\frac{1}{2}} = (\delta f_j - \delta f_{j-1}) - \frac{h_j}{2} [\delta p_j + \delta p_{j-1}] - (f_{j-1} - f_j) - h_j p_{j-\frac{1}{2}}$$

$$p^l = q$$

$$(r_2)_{j-\frac{1}{2}} = (\delta p_j - \delta p_{j-1}) - \frac{h_j}{2} [\delta q_j + \delta q_{j-1}] - (p_{j-1} - p_j) - h_j q_{j-\frac{1}{2}}$$

$$\theta^l = g$$

$$(r_3)_{j-\frac{1}{2}} = (\delta \theta_j - \delta \theta_{j-1}) - \frac{h_j}{2} [\delta g_j + \delta g_{j-1}] - (\theta_{j-1} - \theta_j) - h_j g_{j-\frac{1}{2}}$$

$$\phi^l = \eta$$

$$(r_4)_{j-\frac{1}{2}} = (\delta \phi_j - \delta \phi_{j-1}) - \frac{h_j}{2} [\delta \eta_j + \delta \eta_{j-1}] - (\phi_{j-1} - \phi_j) - h_j \eta_{j-\frac{1}{2}}$$

$$(r_5)_{j-\frac{1}{2}} = (\delta q_{j-1} - \delta q_j) - h_j \left\{ \frac{1}{2} f_{j-\frac{1}{2}} (\delta q_j + \delta q_{j-1}) + \frac{1}{2} q_{j-\frac{1}{2}} [\delta f_j + \delta f_{j-1}] \right\} - h_j \frac{1}{2} G_r (\delta \theta_j + \delta \theta_{j-1}) - h_j \frac{1}{2} G_c (\delta \phi_j + \delta \phi_{j-1}) + 2 h_j p_{j-\frac{1}{2}} (\delta p_j + \delta p_{j-1}) + h_j \frac{1}{2} (M + K) (\delta p_j + \delta p_{j-1})$$

$$(r_6)_{j-\frac{1}{2}} = \left(1 + \frac{4}{3}\right) \left(\delta q_{j-1} - \delta q_j \right) - h_j \text{Pr} \left\{ \frac{1}{2} f_{j-\frac{1}{2}} (\delta g_j + \delta g_{j-1}) + \frac{1}{2} g_{j-\frac{1}{2}} [\delta f_j + \delta f_{j-1}] \right\} + h_j \text{Pr} \frac{1}{2} p_{j-\frac{1}{2}} (\delta \theta_j + \delta \theta_{j-1}) + \frac{1}{2} \theta_{j-\frac{1}{2}} (\delta p_j + \delta p_{j-1}) - h_j \text{Pr } Nb \left\{ \frac{1}{2} g_{j-\frac{1}{2}} (\delta \eta_j + \delta \eta_{j-1}) + \frac{1}{2} \eta_{j-\frac{1}{2}} (\delta g_j + \delta g_{j-1}) \right\} - h_j \text{Pr } Nt \left\{ g_{j-\frac{1}{2}} (\delta g_j + \delta g_{j-1}) \right\} - \frac{1}{2} h_j \text{Pr } Du (\delta \eta_j + \delta \eta_{j-1}) - \frac{h_j}{2} Pr \lambda [A_1 (\delta p_j + \delta p_{j-1}) + B_1 (\delta \theta_j + \delta \theta_{j-1})]$$

$$(r_7)_{j-\frac{1}{2}} = Nb (\delta \eta_j + \delta \eta_{j-1}) + Nt (\delta g_j + \delta g_{j-1}) - h_j Le \text{Pr } Nb \left\{ \frac{1}{2} f_{j-\frac{1}{2}} (\delta \eta_j + \delta \eta_{j-1}) + \frac{1}{2} \eta_{j-\frac{1}{2}} (\delta f_j + \delta f_{j-1}) \right\} + h_j Le \text{Pr } Nb \left\{ \frac{1}{2} p_{j-\frac{1}{2}} (\delta \phi_j + \delta \phi_{j-1}) + \frac{1}{2} \phi_{j-\frac{1}{2}} (\delta p_j + \delta p_{j-1}) \right\} + K_1 Le \text{Pr } Nb \frac{h_j}{2} (\delta \phi_j - \delta \phi_{j-1})$$

With change boundary conditions

$$f(\eta) = S + \lambda(1 - e^{-\eta}), f'(\eta) = \lambda e^{-\eta}$$

$$\theta(\eta) = -\lambda e^{-\eta}, \theta'(\eta) = \lambda e^{-\eta}$$

$$\phi(\eta) = -e^{-\eta}, \phi'(\eta) = e^{-\eta}$$

Program Code Validation:

To validate programme code for verification, Table 1 compares current Nusselt number results with published results by Magyari and Keller [24], Bidin and Nazar [25], El-Aziz [26] and Sharma et al [27] in the absence of Nanofluid, with $S = 0$, $\lambda = 1.5$, and $R = 0$. This table demonstrates that data generated by the new code and the prior code are comparable in quality (Magyari and Keller [24], Bidin and Nazar [25], El-Aziz [26] & Sharma et al [27]).

Table 1. Compares experimentally determined Nusselt numbers to previously published ones to identify variations when $S = 0$, $\lambda = 1.5$, and $R = 0$.

Pr	Keller and Magyari [24]	Nazar and Bidin [25]	El-Aziz [26]	Sharma et al [27]	Present results
1.0	0.9548	0.9547	0.9548	0.954789	0.9546
2.0	-----	1.4714	-----	1.471461	1.4715
3.0	1.8691	1.8691	1.8691	1.869073	1.8692
5.0	2.5001	-----	2.5001	2.500125	2.5000
10.0	3.6604	-----	3.6604	3.660350	3.6601

4. Result and Discussion

The behaviour of the temperature, concentration, and velocity profiles has been carefully examined. Theoretical heat and mass transfer analysis has been carried out using graphical and numerical methods.

As shown in Figures 3-5, the symbol M stands for the magnetic condition and the effect of the magnetic field on temperature, concentration, and velocity. A transverse magnetic field causes the Lorentz force, which in turn produces a force that retards velocity movement. When the temperature and concentration profiles grow, the velocity decreases because the retarding force increases with the value of M . Notably, the solutal concentration profile is lowered farther from the sheet due to the significant magnetic strength. The impact of the suction/injection parameter (S) on the dimensionless stream-wise velocities (V) is shown in Figure 6. The graphs in Figure 6 show that the parameter S has a significant impact on the boundary layer's thickness. As S is raised, the flow seems to drastically slow down. The boundary layer is forced closer to the wall by suction or injection, which lowers velocity. The suction/injection causes a reduction in the thickness of the momentum boundary layer. The ratio λ describes the stretching speeds between the two directions, y , x . The stretching rate ratio parameter increases when the y -direction velocity increases and the x -direction velocity decreases, as shown in Figure 7. The temperature profile seen in Figure 8 is initiated by the Prandtl number. As the Prandtl number continuously increases, the thermal diffusivity weakens and the thermal boundary layer thins. Figure 9 depicts the impact of thermal radiation parameter R on the temperature field. The profile of temperature increases as a function of R . The thickness of the thermal boundary layer is improved by an increase in the thermal radiation parameter. The temperature and concentration graphs fluctuate in response to variations in the Brownian motion parameter Nb , as shown in Figures 10 and 11. The concentration profile graph and temperature are influenced by Brownian motion in that when the parameter values rise, the concentration boundary layer thickness decreases and the temperature rises. The graph also shows that as Nb values rise,

the thermal boundary layer thickness does not vary significantly. Figures 12 and 13 illustrate how changes in the thermophoresis parameter Nt cause fluctuations in the temperature and concentration graphs. The temperature drops and the concentration rises as the Nt values rise. The effect of the Lewis number on the volume concentration of dimensionless nanoparticles is seen in Figure 14. We find that for larger Le values, there is a significant decrease in the nanoparticle volume fraction. The ratio of heat to mass diffusivity is the definition of the dimensionless Lewis number. The thickness of the thermal boundary layer increases while the thickness of the boundary layer containing the volume concentration of nanoparticles decreases when Le is increased. in Figures 15-17 Grashof number rises with increasing velocity profile. Increased values of Grashof number induce an augmentation in shrinking forces, which in turn causes an increase in fluid flow. As the Gr numbers rise, the concentration and temperature decrease. From The Grashof Number for mass transfer is illustrated in Figures 18-20. As Gc increases, concentration, temperature, and velocity values decrease.

Figure 21 shows the impact of various permeability parameter values on velocity fields. It is evident that a porous media increases the restriction on the fluid flow, slowing the fluid's velocity. when a result, when the permeability parameter increases, so does the resistance to fluid motion, which causes a decrease in velocity. The behaviour of the non-uniform heat source on temperature distributions is seen in Figure 22. The figure makes it clear that improving the non-uniform heat source settings improves the temperature profiles. This validates the heat source's overall physical behaviour, which shows that positive values for $A1$ and $B1$ function as heat generators. The thickness of the thermal boundary layer generally increases with an increase in the heat source. Figure 23 illustrates how different values of the DuFour number Du affect the heat profile. It is evident that the temperature profile is significantly impacted by Du . It has been discovered that an increase in the Du causes the temperature of the boundary layer as a whole to rise and then gradually decrease from the surface to the free flow value. The concentration distribution for the DuFour parameter is displayed in Figure 24, which indicates that concentration grows

steadily as Du increases. Figure 25 shows the influence of the chemical reaction parameter (Kr) on the temperature field. A rise in the thermal boundary layer is observed with an increase in the chemical reaction parameter. The thermal boundary

layer's change with the chemical reaction parameter (Kr) is depicted in Figure 26. It is found that as the chemical reaction parameter increases, the thickness of the thermal boundary layer decreases.

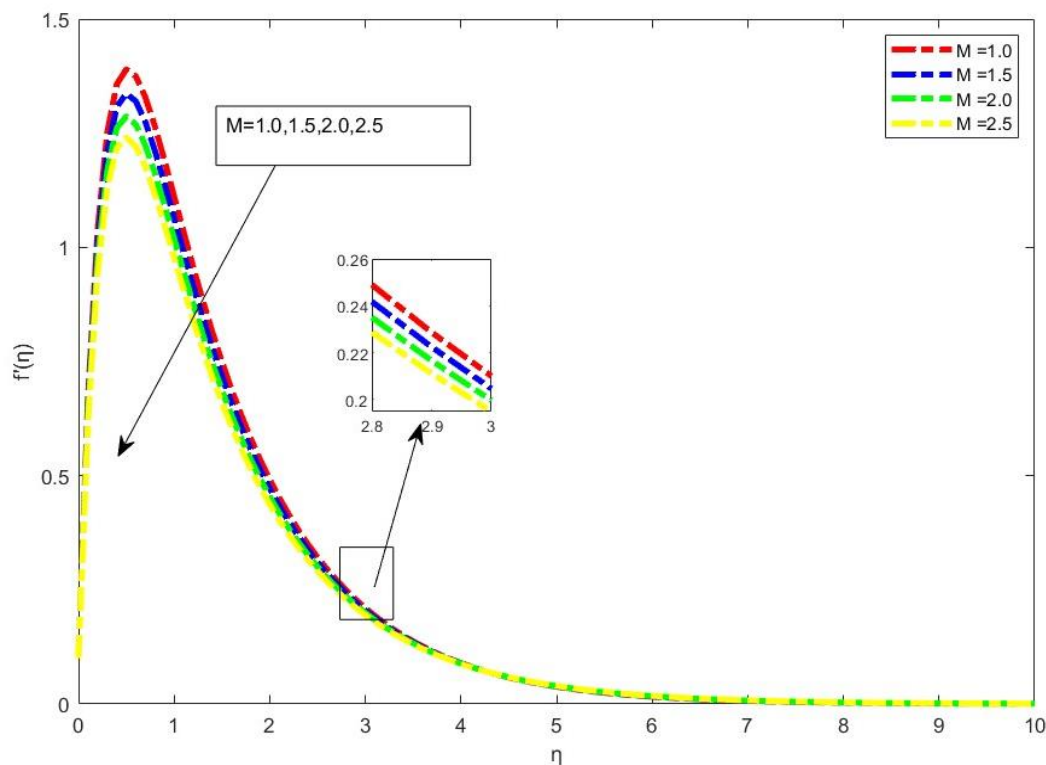


Figure 3. Impact of M on Velocity.

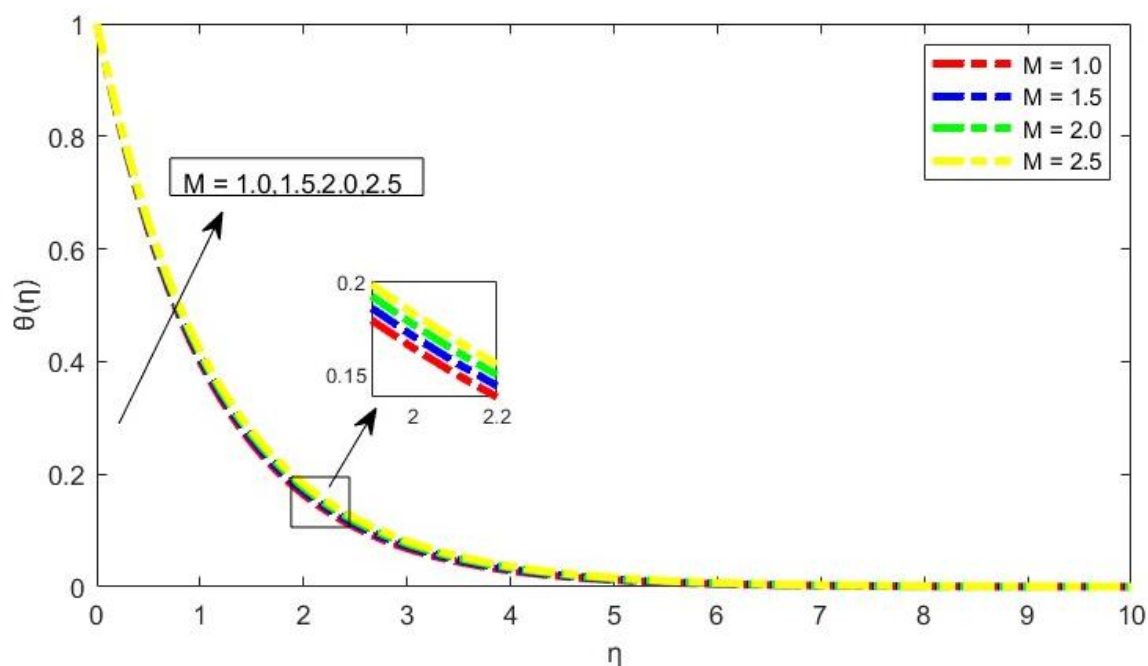


Figure 4. Impact of M on Temperature.

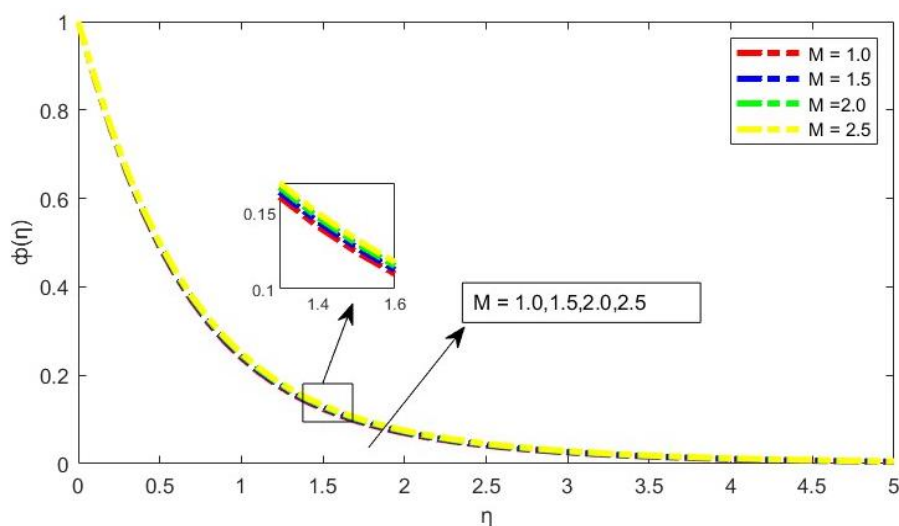


Figure 5. Impact of M on Concentration.

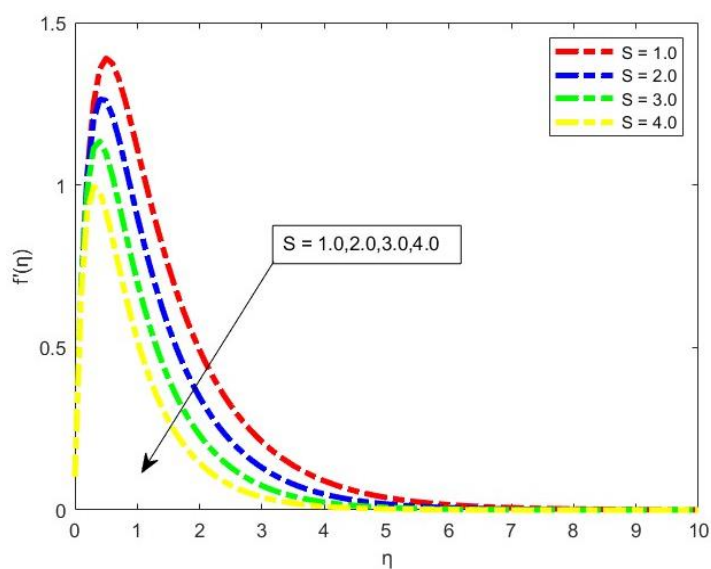


Figure 6. Impact of S on Velocity.

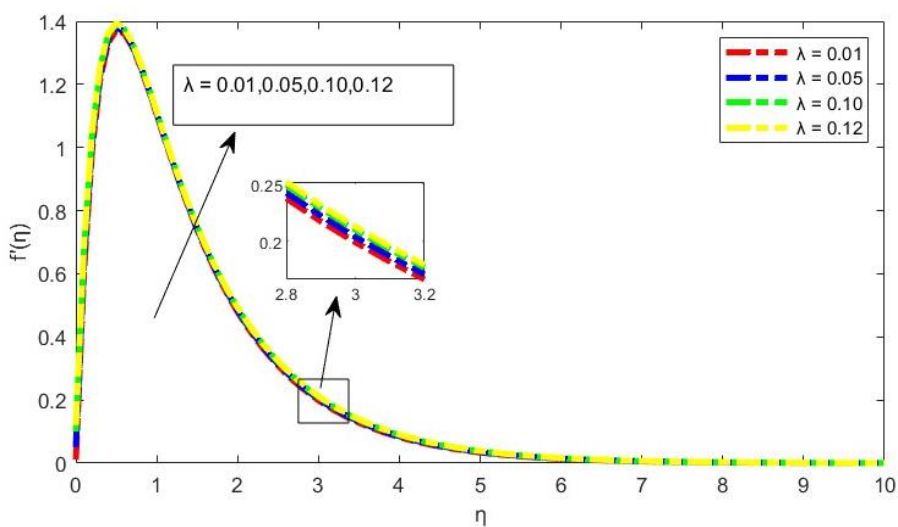


Figure 7. Impact of λ on Velocity.

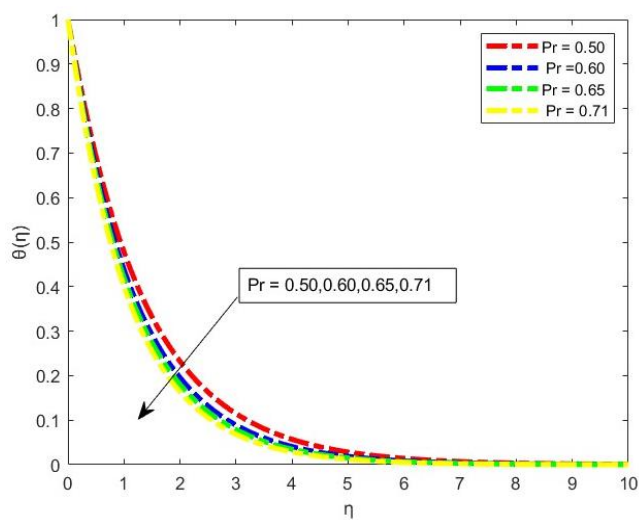


Figure 8. Impact of Pr on Temperature.

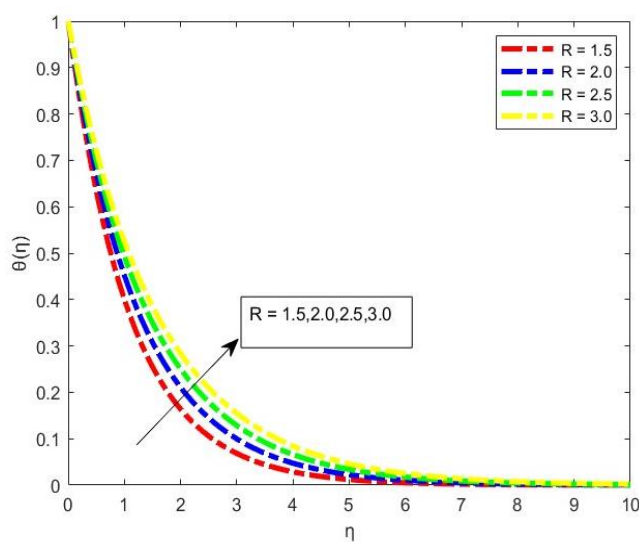


Figure 9. Impact of R on Temperature.

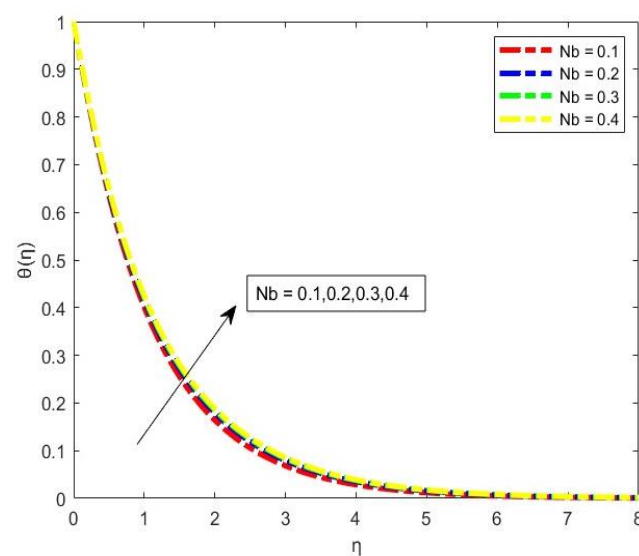


Figure 10. Impact of Nb on Temperature.

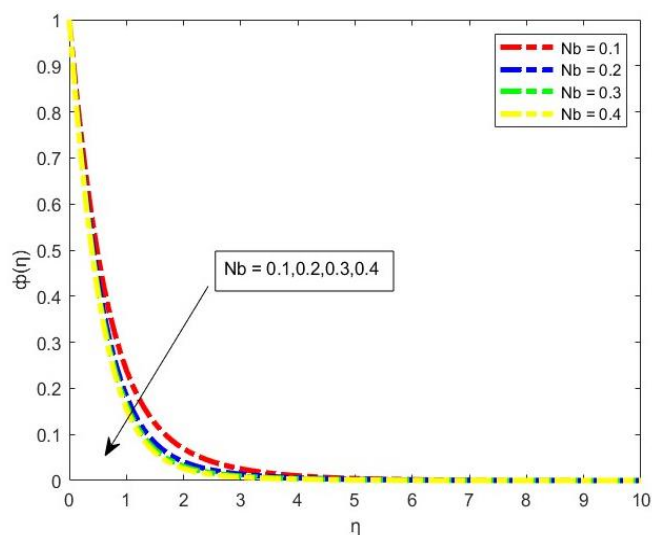


Figure 11. Impact of Nb on Concentration.

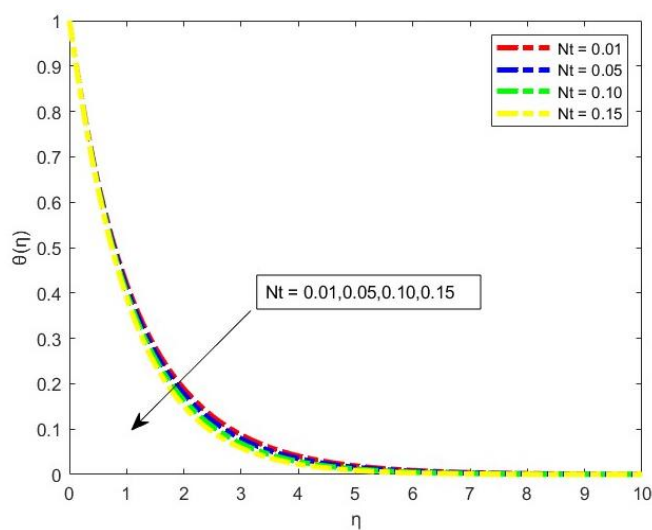


Figure 12. Impact of Nt on Temperature.

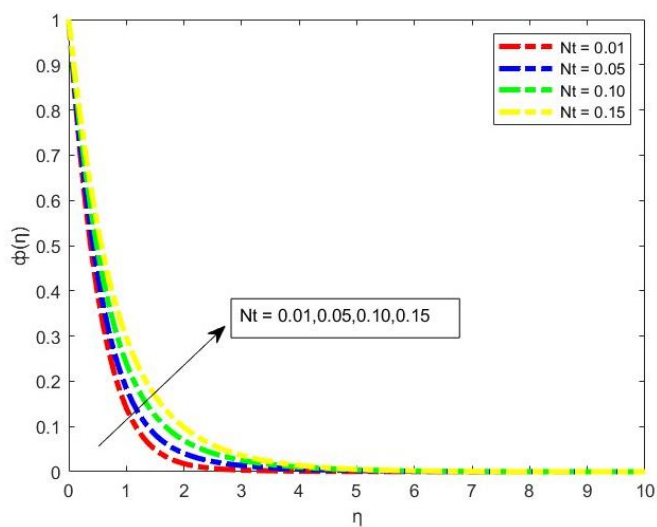


Figure 13. Impact of Nt on Concentration.

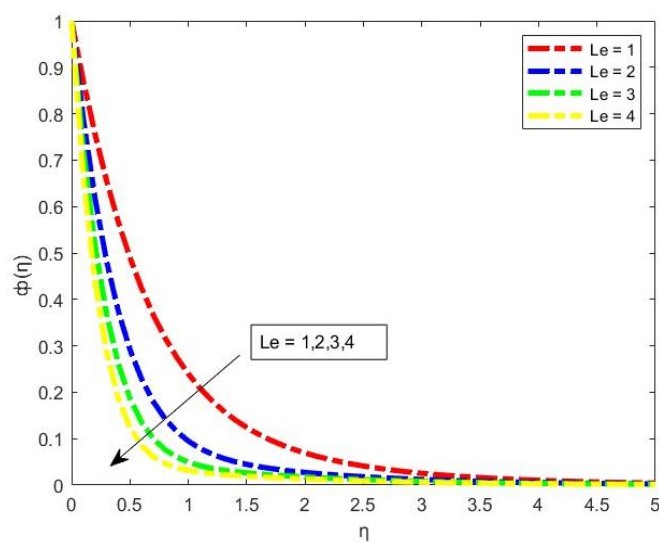


Figure 14. Impact of Le on Concentration.

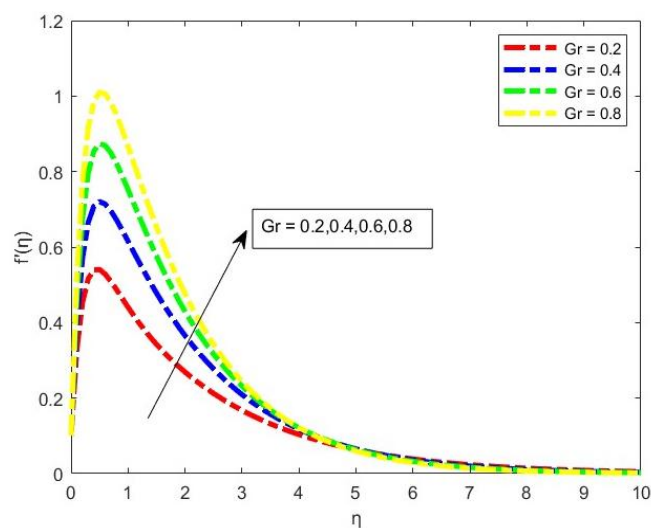


Figure 15. Impact of Gr on Velocity.

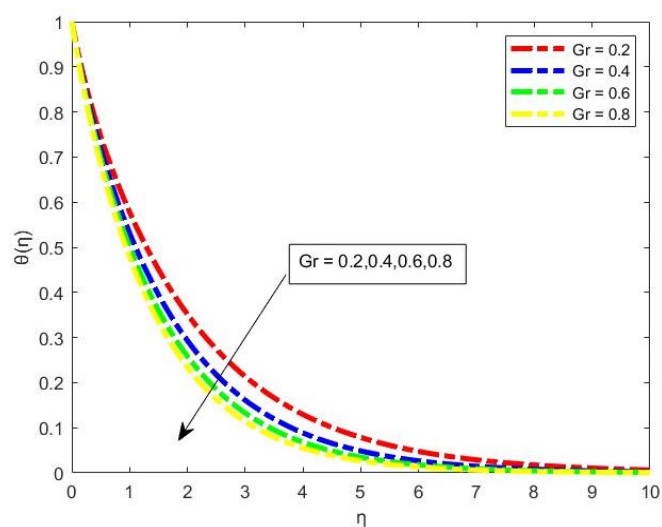


Figure 16. Impact of Gr on Temperature.

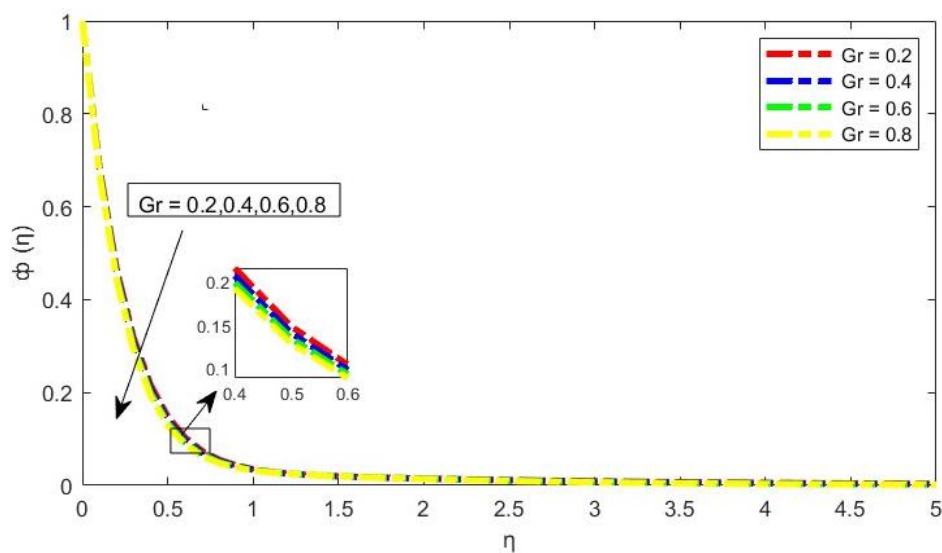


Figure 17. Impact of Gr on Concentration.

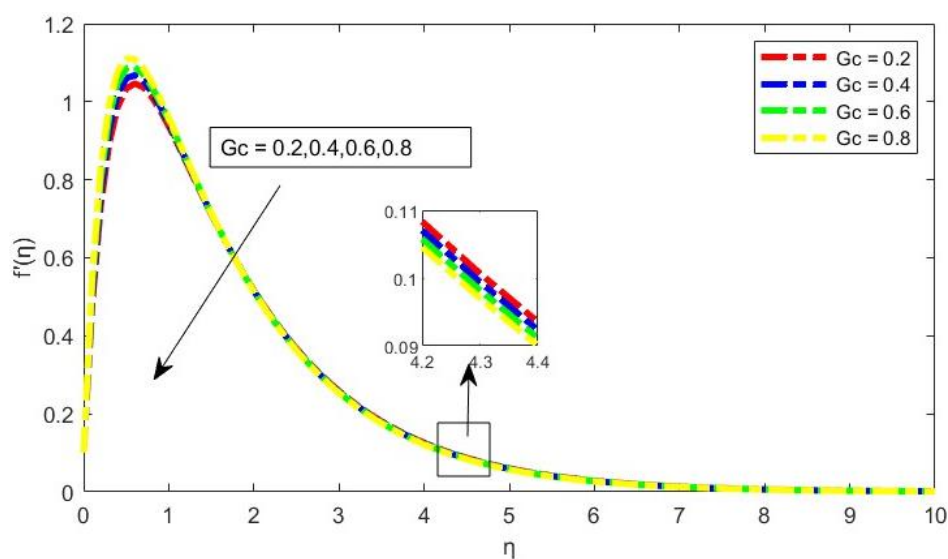


Figure 18. Impact of Gc on Velocity.

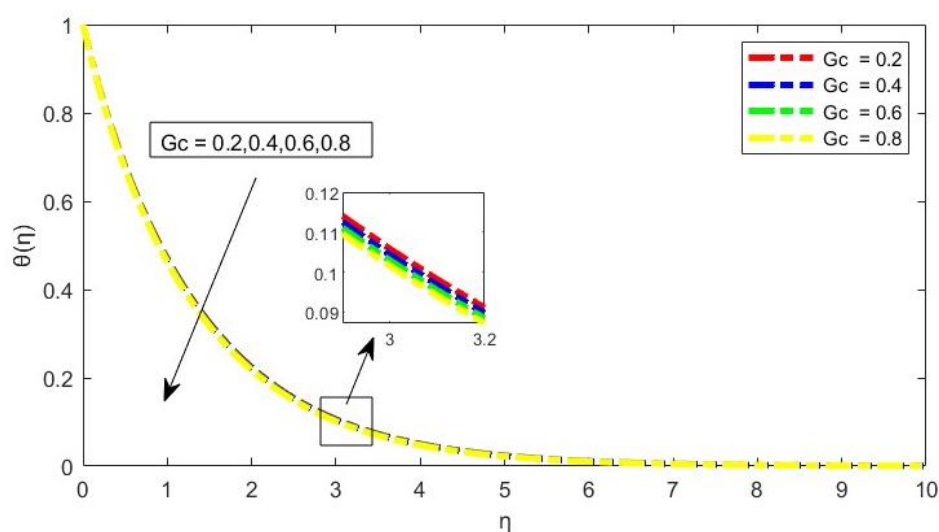


Figure 19. Impact of Gc on Temperature.

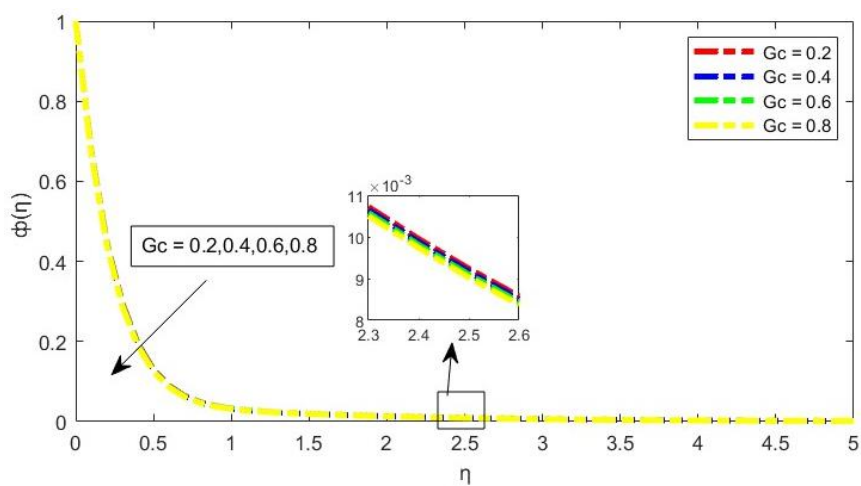


Figure 20. Impact of G_c on Concentration.

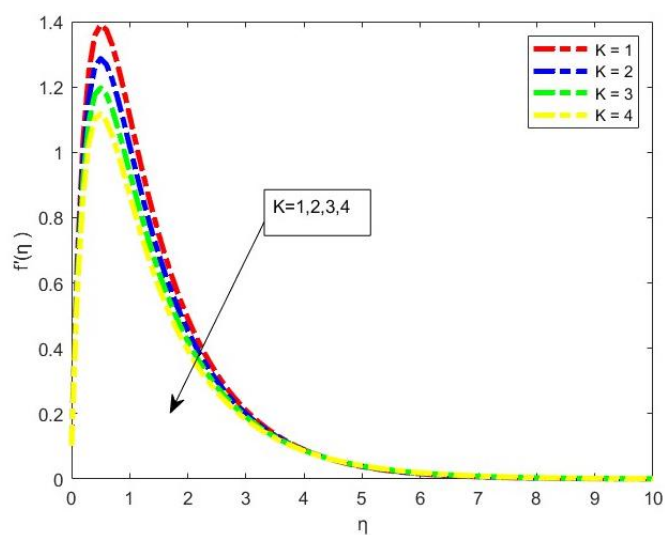


Figure 21. Impact of K on Velocity.

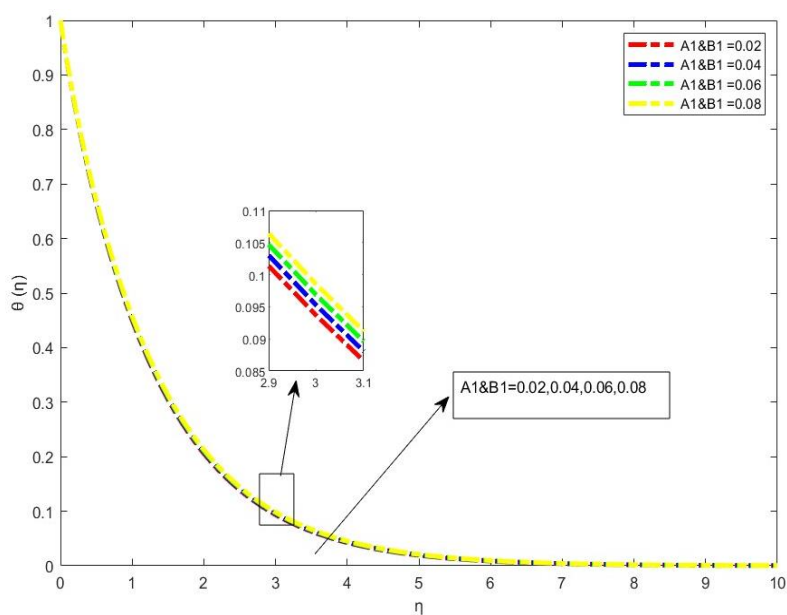


Figure 22. Impact of A_1 & B_1 on Temperature.

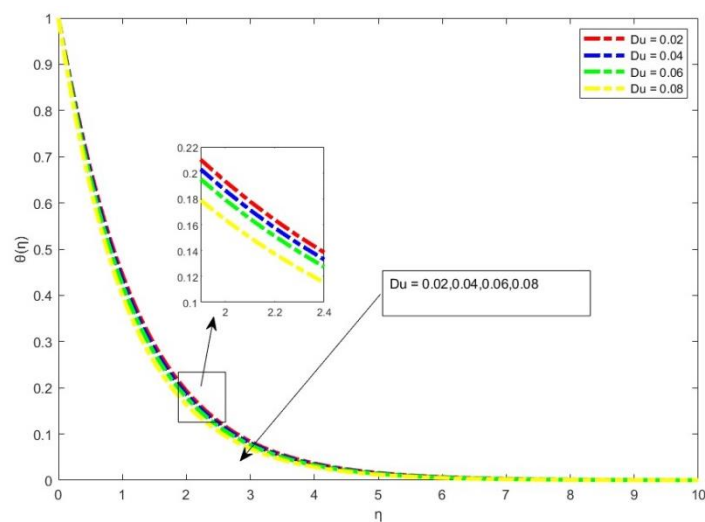


Figure 23. Impact of Du on Temperature.

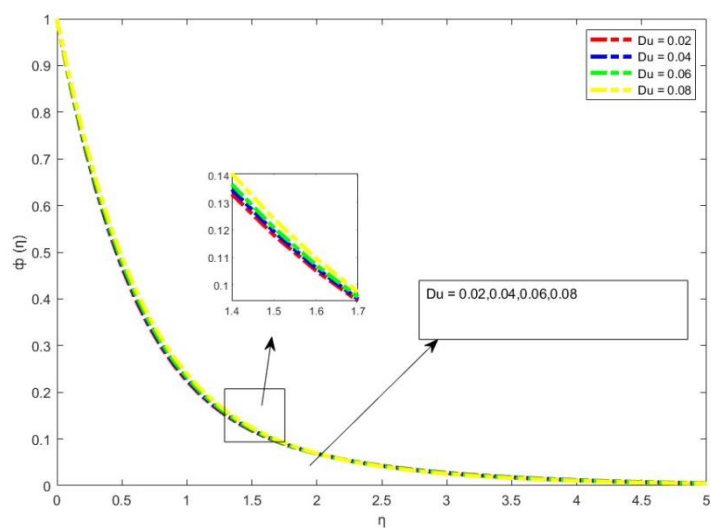


Figure 24. Impact of Du on Concentration.

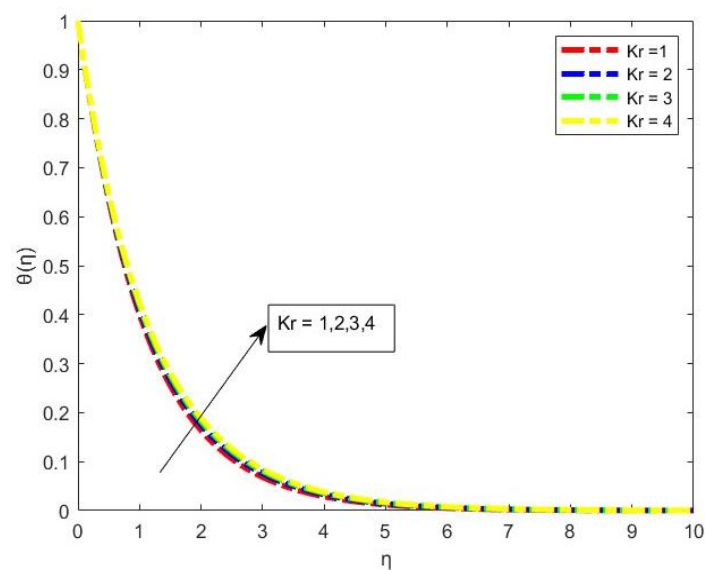


Figure 25. Impact of Kr on Temperature.

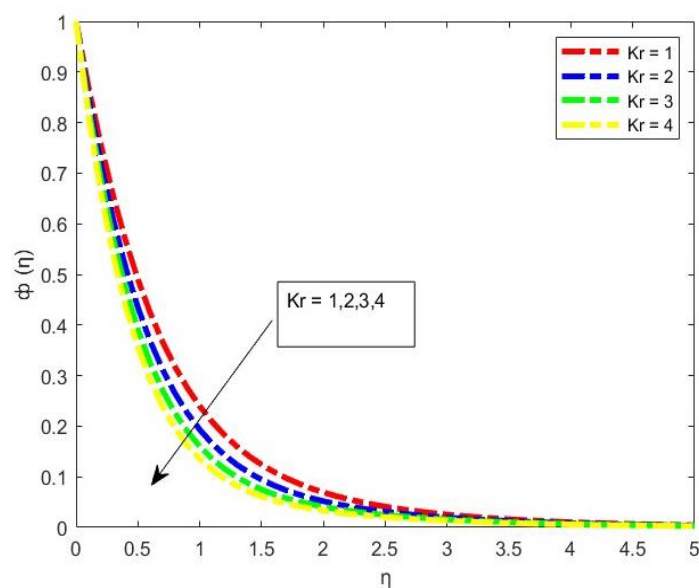


Figure 26. Impact of K_r on Concentration.

Table 2. Calculation of the skin friction coefficient for different values M , Gr , Gc , R , S , λ and K .

M	Gr	Gc	R	S	λ	K	Cf_x
1.0							2.1720
2.0							1.6116
3.0							1.0952
4.0							0.6168
	0.2						0.2098
	0.4						0.4201
	0.6						1.0234
	0.8						1.6061
		0.2					0.1943
		0.4					0.7016
		0.6					1.1999
		0.8					1.6898
			1.5				2.1720
			2.0				2.2511
			2.5				2.3127
			3.0				2.3625
				1.0			2.1720
				2.0			1.7460
				3.0			1.0363
				4.0			0.0245
					1.0		3.9760
					1.5		2.1720

M	Gr	Gc	R	S	λ	K	Cf _x
					2.0		0.2455
					2.5		-1.7972
						1.0	2.1720
						2.0	1.6116
						3.0	1.0952
						4.0	0.6168

Table 3. Calculation of the Local share wood number for different values M, Gr, Gc, Nb, Nt, Du, Kr and Le.

M	Gr	Gc	Nb	Nt	Du	Kr	Le	Sh _x
1.0								1.5180
2.0								1.4994
3.0								1.4825
4.0								1.4673
	0.2							1.4434
	0.4							1.4643
	0.6							1.4836
	0.8							1.5014
		0.2						1.4667
		0.4						1.4803
		0.6						1.4934
		0.8						1.5060
			0.1					1.5180
			0.2					1.7483
			0.3					1.8265
			0.4					1.8660
				0.1				1.5180
				0.2				1.0965
				0.3				0.7105
				0.4				0.3619
					0.02			1.6290
					0.04			1.6011
					0.06			1.5732
					0.08			1.5456
						1.0		1.5180
						2.0		1.4994
						3.0		1.9646
						4.0		2.1573

M	Gr	Gc	Nb	Nt	Du	Kr	Le	Sh _x
							1.0	1.4994
							2.0	2.6342
							3.0	3.6132
							4.0	4.5212

Table 4. Heat transfer rate coefficients for various values of M , Pr , Nb , Nt , Gr , Gc , Du , Kr and $A1 \& B1$.

M	Gr	Gc	Pr	Nb	Nt	R	Du	Kr	A1&B1	Nu _x
1.0										0.9358
2.0										0.9154
3.0										0.8942
4.0										0.8746
	1.0									0.9385
	0.8									0.9181
	0.5									0.8826
	0.2									0.8374
		1.0								0.9385
		0.8								0.9252
		0.5								0.9038
		0.2								0.8803
			0.71							0.9385
			0.81							1.0476
			0.91							1.1315
			1.0							1.1681
				0.1						0.9385
				0.2						0.9212
				0.3						0.9074
				0.4						0.8946
					0.1					0.9385
					0.2					0.9402
					0.3					0.9830
					0.4					1.0009
						1.5				0.9385
						2.0				0.8268
						2.5				0.7582
						3.0				0.6925
								0.01		0.7855
								0.02		0.8026

M	Gr	Gc	Pr	Nb	Nt	R	Du	Kr	A1&B1	Nu _x
							0.04			0.8367
							0.06			0.8708
								1.0		0.9385
								2.0		0.9346
								3.0		0.9317
								4.0		0.9296
									0.01	0.9385
									0.02	0.9038
									0.04	0.8486
									0.06	0.5617

Table 2 provides skin friction values for M , Gr , Gc , R , S , λ , and K . We see that as we increase the values of Gr and R , skin friction also increases, but in other circumstances it decreases.

Table 3 shows the local share wood values for M , Gr , Gc , Nb , Nt , Du , Kr , and Le . We can observe that as we increase the values of Gr , Gc , Nb , and Le , the share wood number grows, but in other cases it falls.

Table 4 displays the local Nusselt numbers (heat transfer) for M , Gr , Gc , Nb , Nt , Pr , R , Du , Kr , and $A1&B1$. We can see that as we increase the parameters Pr , Nt , and Du , the nusselt number increases whereas in other cases it decreases.

5. Conclusion

The effects of thermal diffusion (Soret) and diffusion-thermo (DuFour) on MHD mixed convective flow of a viscous nanofluid across a stretching sheet in the presence of a non-uniform heat source/sink and a chemical reaction embedded in a porous media under a magnetic field were investigated. The results are refined using a numerical technique known as the Keller box technique. The following points summarise the study's main findings.

- 1) Velocity profiles grow with stretching sheet parameter values and reverse trend is observed for permeability parameter.
- 2) Rising suction/injection parameters (S) and magnetic field parameters (M) cause a drop in the velocity profile.
- 3) As thermal radiation increases, the temperature profile also rises.
- 4) Temperature profiles decrease as the Prandtl number (Pr) value increases.
- 5) The Brownian motion parameter (Nb) value is growing, as is the temperature, while the concentration profiles are following the opposite pattern.
- 6) The thermophoresis parameter (Nt) value is growing, while temperature is falling, and concentration profiles

are in reverse.

- 7) The value of the Lewis parameter (Le) is increasing The concentration is falling.
- 8) Thermal Grashof number (Gr) is increasing, velocity is increasing, and temperature and concentration are on the reverse trend.
- 9) The concentration, temperature, and velocity values drop as the Concentration Grashof number (Gc) increases.
- 10) Temperature was found to rise as the space-dependent ($A1$) and temperature-dependent ($B1$) parameters for heat source/sink increased.
- 11) Increasing Du values leads to a decrease in temperature, while concentration profiles show the opposite.
- 12) Chemical reaction parameter Kr values increase as temperature rises, while the concentration profile decreases.

Abbreviations

u_w, v_w	Velocity Components Along x,y Axis
M	Magnetic Field
τ_B	Ratio of the Heat Capacity of Nanoparticle & Heat Capacity of the Base Fluid
D_T	Thermophoresis Coefficient
λ	Stretching Parameter
S	Suction /Injection Parameter
Pr	Prandtl Number
Nb	Brownian Motion Parameter
Φ	Fluid Concentration
θ_w	Wall Temperature
K	Porosity
G_c	Grashof Number Species Concentration
B_1	Space Dependent Variable
Nt	Thermophoresis Parameter
Le	Lewis Number

K_r	Chemical Reaction
ρ	Fluid Density
D_B	Brownian Coefficient
R	Thermal Radiation Parameter
Du	DuFour Effect
θ	Fluid Temperature
α	Inclined Angle
ϕ_w	Wall Concentration
G_r	Grashof Number Due to Temperature
A_1	Time Dependent Variable
c_p	Specific Heat

Author Contributions

Prashanth: Conceptualization, Data curation, Formal Analysis, Investigation, Methodology, Resources, Software, Validation, Visualization, Writing – original draft, Writing – review & editing

Srinivasa Rao: Supervision, Visualization, Writing – review & editing

Conflicts of Interest

The authors declare no conflicts of interest.

References

- [1] Crane, L. J., 1970. Flow past a stretching plate. *Zeitschrift für angewandte Mathematik und Physik ZAMP*, 21, pp. 645-647. <https://doi.org/10.1007/BF01587695>
- [2] Takhar, H. S., Chamkha, A. J. and Nath, G., 2000. Flow and mass transfer on a stretching sheet with a magnetic field and chemically reactive species. *International Journal of Engineering Science*, 38(12), pp. 1303-1314. [https://doi.org/10.1016/S0020-7225\(99\)00079-8](https://doi.org/10.1016/S0020-7225(99)00079-8)
- [3] Hayat, T. and Javed, T., 2007. On analytic solution for generalized three-dimensional MHD flow over a porous stretching sheet. *Physics Letters A*, 370(3-4), pp. 243-250. <https://doi.org/10.1016/j.physleta.2007.05.108>
- [4] Krishnaiah, M., Rajendar, P., Laxmi, T. V. and Reddy, M. C. K., 2017. Influence of non-uniform heat source/sink on stagnation point flow of a MHD Casson nanofluid flow over an exponentially stretching surface. *Glob J Pure Appl Math*, 13, pp. 7009-7033.
- [5] Konda, J. R., NP, M. R., Konijeti, R. and Dasore, A., 2019. Effect of non-uniform heat source/sink on MHD boundary layer flow and melting heat transfer of Williamson nanofluid in porous medium. *Multidiscipline Modeling in Materials and Structures*, 15(2), pp. 452-472. <https://doi.org/10.1108/MMS-01-2018-0011>
- [6] Gangadhar, K. and Suneetha, S., 2015. Soret and DuFour effects on MHD free convection flow of a chemically reacting fluid past over a stretching sheet with heat source/sink. *Open Science Journal of Mathematics and Application*, 3(5), pp. 136-146.
- [7] Pal, D. and Mondal, H., 2013. Influence of Soret and DuFour on MHD buoyancy-driven heat and mass transfer over a stretching sheet in porous media with temperature-dependent viscosity. *Nuclear Engineering and Design*, 256, pp. 350-357. <https://doi.org/10.1016/j.nucengdes.2012.08.015>
- [8] Patil, P. M. and Kumbarwadi, N., 2018. Effects of MHD mixed convection with non-uniform heat source/sink and cross-diffusion over exponentially stretching sheet. *International Journal of Numerical Methods for Heat & Fluid Flow*, 28(6), pp. 1238-1255. <https://doi.org/10.1108/HFF-04-2017-0149>
- [9] Thumma, T. and Mishra, S. R., 2020. Effect of nonuniform heat source/sink, and viscous and Joule dissipation on 3D Eyring–Powell nanofluid flow over a stretching sheet. *Journal of Computational Design and Engineering*, 7(4), pp. 412-426. <https://doi.org/10.1093/jcde/qwaa034>
- [10] Karim, M. E., Samad, M. A. and Hasan, M. M., 2012. DuFour and Soret effect on steady MHD flow in presence of Heat generation and magnetic field past an inclined stretching sheet. <https://doi.org/10.4236/ojfd.2012.23009>
- [11] Mondal, H., Pal, D., Chatterjee, S. and Sibanda, P., 2018. Thermophoresis and Soret-DuFour on MHD mixed convection mass transfer over an inclined plate with non-uniform heat source/sink and chemical reaction. *Ain Shams Engineering Journal*, 9(4), pp. 2111-2121. <https://doi.org/10.1016/j.asej.2016.10.015>
- [12] Kalyani, C., Reddy, M. C. K. and Kishan, N., 2015. MHD mixed convection flow past a vertical porous plate in a porous medium with heat source/sink and soret effects. *American Chemical Science Journal*, 7(3), pp. 150-159.
- [13] Aastha, A. and Chand, K., 2023. Soret and DuFour Effects on Chemically Reacting and Viscous Dissipating Nanofluid Flowing Past a Moving Porous Plate in the Presence of a Heat Source/Sink. *Acta Mechanica et Automatica*, 17(2), pp. 263-271. <https://doi.org/10.2478/ama-2023-0030>
- [14] Ramadevi, B., Kumar, K. A., Sugunamma, V. and Sandeep, N., 2019. Influence of non-uniform heat source/sink on the three-dimensional magnetohydrodynamic Carreau fluid flow past a stretching surface with modified Fourier's law. *Pramana*, 93, pp. 1-11. <https://doi.org/10.1007/s12043-019-1847-7>
- [15] Hayat, T., Asad, S. and Alsaedi, A., 2017. Non-uniform heat source/sink and thermal radiation effects on the stretched flow of cylinder in a thermally stratified medium. *Journal of Applied Fluid Mechanics*, 10(3), pp. 915-924. <https://doi.org/10.18869/acadpub.jafm.73.240.24008>
- [16] Ali, M. and Alam, M. S., 2014. Soret and Hall effect on MHD flow heat and mass transfer over a vertical stretching sheet in a porous medium due to heat generation. *ARP Journal of Engineering and Applied Science*, 9(3).
- [17] Seth, G. S., Tripathi, R. and Rashidi, M. M., 2017. Hydro-magnetic natural convection flow in a non-Darcy medium with Soret and DuFour effects past an inclined stretching sheet. *Journal of Porous Media*, 20(10). <https://doi.org/10.1615/JPorMedia.v20.i10.50>

- [18] Sheikh, M. and Abbas, Z., 2015. Effects of thermophoresis and heat generation/absorption on MHD flow due to an oscillatory stretching sheet with chemically reactive species. *Journal of Magnetism and Magnetic Materials*, 396, pp. 204-213 <https://doi.org/10.1016/j.jmmm.2015.08.011>
- [19] Reddy, P. S. and Chamkha, A. J., 2016. Soret and DuFour effects on MHD convective flow of Al_2O_3 -water and TiO_2 -water nanofluids past a stretching sheet in porous media with heat generation/absorption. *Advanced Powder Technology*, 27(4), pp. 1207-1218. <https://doi.org/10.1016/j.appt.2016.04.005>
- [20] Ragupathi, P., Hakeem, A. A., Al-Mdallal, Q. M., Ganga, B. and Saranya, S., 2019. Non-uniform heat source/sink effects on the three-dimensional flow of $\text{Fe}_3\text{O}_4/\text{Al}_2\text{O}_3$ nanoparticles with different base fluids past a Riga plate. *Case Studies in Thermal Engineering*, 15, p. 100521. <https://doi.org/10.1016/j.csite.2019.100521>
- [21] Koli, C. M. and Salunkhe, S. N., 2023. Thermal Radiation and Magnetic Fields Effects on Nanofluids flowing through Stretch Sheet. *Journal of Computational Applied Mechanics*, 54(1), pp. 111-126. <https://doi.org/10.22059/jcamech.2023.353492.791>
- [22] Lakshmi, B. K., Sugunamma, V. and Reddy, J. R., 2018. Soret and DuFour effects on MHD flow of Sisko fluid over a stretching sheet with non-uniform heat source/sink. *Int J Emerg Technol Eng Res*, 6(2), pp. 125-136.
- [23] Reddy, P. S., Sreedevi, P. and Chamkha, A. J., 2023. Hybrid nanofluid heat and mass transfer characteristics over a stretching/shrinking sheet with slip effects. *Journal of Nanofluids*, 12(1), pp. 251-260. <https://doi.org/10.1166/jon.2023.1996>
- [24] Magyari, E. and Keller, B., 1999. Heat and mass transfer in the boundary layers on an exponentially stretching continuous surface. *Journal of Physics D: Applied Physics*, 32(5), p. 577 <https://doi.org/10.1088/0022-3727/32/5/012>
- [25] Bidin, B. and Nazar, R., 2009. Numerical solution of the boundary layer flow over an exponentially stretching sheet with thermal radiation. *European journal of scientific research*, 33(4), pp. 710-717.
- [26] Abd El-Aziz, M., 2009. Viscous dissipation effect on mixed convection flow of a micropolar fluid over an exponentially stretching sheet. *Canadian Journal of Physics*, 87(4), pp. 359-368. <https://doi.org/10.1139/P09-047>
- [27] Sharma, R., Ishak, A., Nazar, R. and Pop, I., 2014. Boundary layer flow and heat transfer over a permeable exponentially shrinking sheet in the presence of thermal radiation and partial slip. *Journal of Applied Fluid Mechanics*, 7(1), pp. 125-134.